Supplementary information

A GSH-scavenging and synthesis-blocking microneedle patch for augmenting photodynamic eradication of diabetic wound biofilm

Haixia Zhang,[a#] Zhichao Ran,[a#] Yi Li,[a] Jiaying Liu,[d] Hangyu Wang,[e] Junpei Mei,[a] Peihang Song,[a] Wenwei Liu,[a] Chaoqun Liu,[*a,d] Kelei Guan,[*c] Ningning Song[*b]

[a] School of Pharmacy, Henan University, Kaifeng 475004, China.

[b] National & Local Joint Engineering Research Center for Applied Technology of Hybrid Nanomaterials, Henan University, Kaifeng 475004, China.

[c] Department of pharmacy, the First Affiliated Hospital of Zhengzhou University, Zhengzhou 450000, China.

[d] Department of Pharmacy, the First Affiliated Hospital of Henan University, Kaifeng 475001, China.

[e] Department of Gastroenterology, the First Affiliated Hospital of Henan University, Kaifeng 475001, China

[#] These authors contributed equally to this work.

*** Corresponding authors.**

E-mail addresses: cqliu@henu.edu.cn (C. Liu), guankelei2009@126.com (K. Guan), songning@henu.edu.cn (N. Song).

1.1 Materials

Copper nitrate trihydrate (≥99%), tetrakis (4-carboxyphenyl) porphyrin (TCPP, ≥97%), L-buthionine sulfoximine (BSO, ≥95%), methanol (≥99.9%), acetonitrile (≥99.9%), reduced glutathione (GSH, ≥98%), and 5,5′-dithiobis (2-nitrobenzoic acid) (DTNB, ≥98%) were obtained from Aladdin Chemistry Co., Ltd. (Shanghai, China). Polyvinylpyrrolidone K30 (≥99.8%) was purchased from Sinopharm Chemical Reagent Co., Ltd. Fluorescein diacetate (FDA) and propidium iodide (PI) were purchased from Solarbio Technology Co., Ltd. (Beijing, China). Hyaluronic acid (HA, 50 kDa, ≥95%) was provided by Bloomage Biotechnology Co., Ltd. (Jinan, China). The microneedle molds were supplied by Micro-Nano Microchip Pharmaceutical Technology Co., Ltd. Nutrient agar, trypticase soy broth (TSB) and Dulbecco's modified eagle medium (DMEM) were obtained from Aoboxing Biotechnology (Beijing, China). Reactive oxygen species detection probe (DCFH-DA) was purchased from Beyotime Biotechnology Co., Ltd. Streptozotocin (STZ, ≥98.5%) was purchased from Shanghai Yuanye Bio-Technology Co., Ltd. *Staphylococcus aureus* (*S. aureus*) (ATCC 25923) and *Escherichia coli* (*E. coli*) (ATCC 25922) strains were provided by Chuanxiang Biotechnology Co., Ltd. (Shanghai, China).

1.2 Instrumentation

Scanning electron microscopy (SEM) images were captured by a Hitachi S-4800 FESEM. Transmission electron microscopy (TEM) images were obtained using a TEM system (FEI Tecnai G2 F20) with an accelerating voltage of 100 keV. Atomic force microscopy (AFM) analysis was conducted using an instrument from Oxford Instruments Asylum Research Inc. X-ray diffraction (XRD) patterns were obtained using a Bruker D8 Advance diffractometer equipped with Cu Kα radiation. The UV-Vis spectra were measured using a Shimadzu UV-2600 UV-Vis spectrophotometer. Fourier transform infrared (FTIR) spectra were obtained via a Bruker Vertex 70 spectrometer using the KBr pellet method. Surface charge (Zeta) properties and hydrodynamic size distribution (Size) were analyzed using a Malvern Zetasizer Nano ZS90. In addition, the loading capacity and release profile of BSO were directly determined by a High-Performance Liquid Chromatograph (HPLC, Agilent 1260-Infinity II model). Fluorescence imaging was captured using an Olympus BX-51 fluorescence microscope. Three-dimensional fluorescence imaging was obtained using a Nikon AXR laser

scanning confocal microscope. The mechanical properties of the MNs were measured using a Texture Analyzer (FTC TMS-Pro). Finally, *in vivo* fluorescence imaging system data were acquired using an IVIS Lumina XRMS Series device.

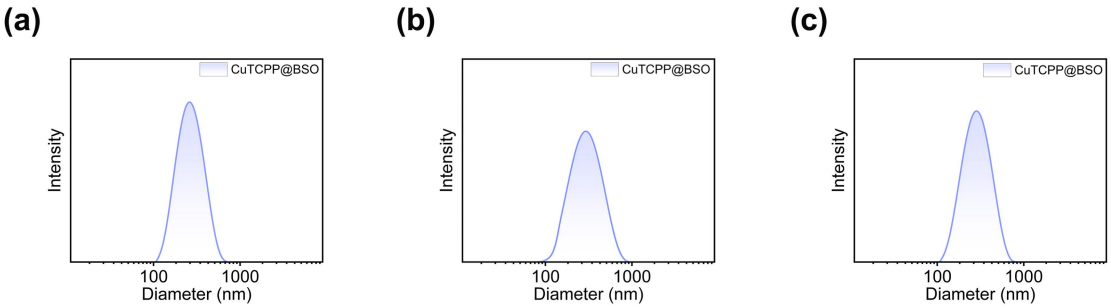

Fig. S1. Hydrodynamic diameter distribution of CuTCPP@BSO dispersed in deionized water after incubation at 37°C for (a) 24 h, (b) 48 h and (c) 72 h.

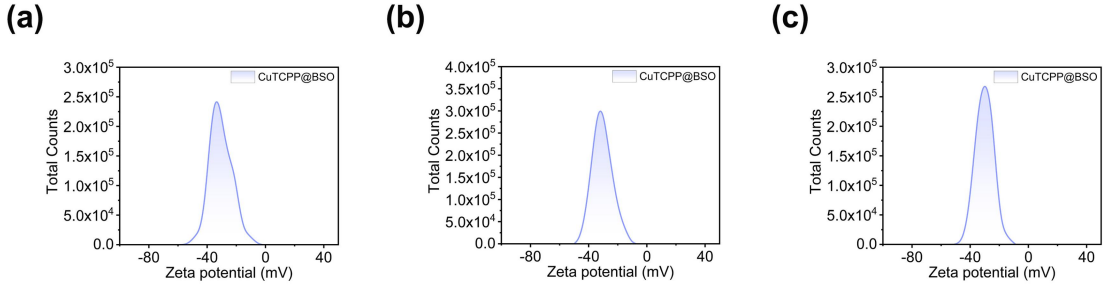

Fig. S2. Zeta potential of CuTCPP@BSO dispersed in deionized water after incubation at 37°C for (a) 24 h, (b) 48 h and (c) 72 h.

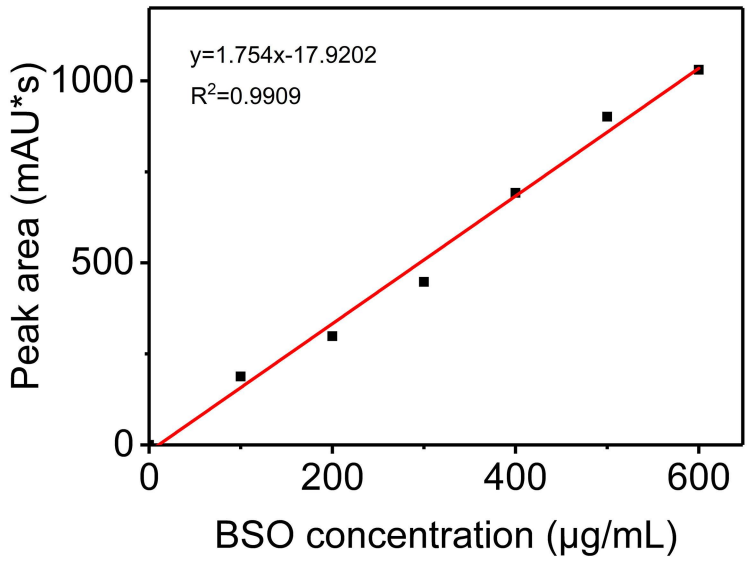

Fig. S3 Standard curve of BSO as determined by HPLC.

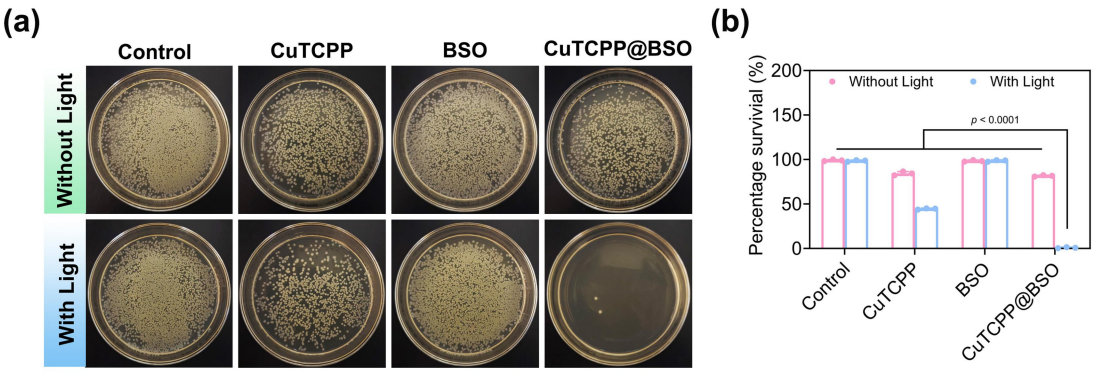

Fig. S4. Antibacterial performance of CuTCPP@BSO against a mixed culture of *S. aureus* and *E. coli*. (a) Representative photographs of bacterial colonies on agar plates post-treatment. (b) Quantitative survival rates calculated from the plate counts in (a).

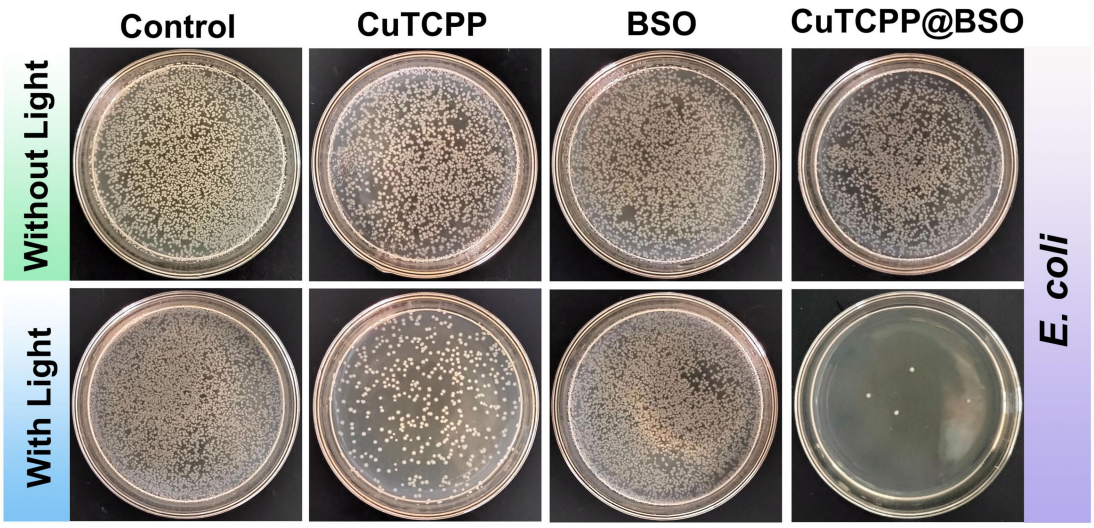

Fig. S5 Photographs of agar plates depicting *E. coli* colony formation after exposure to different therapeutic regimens.

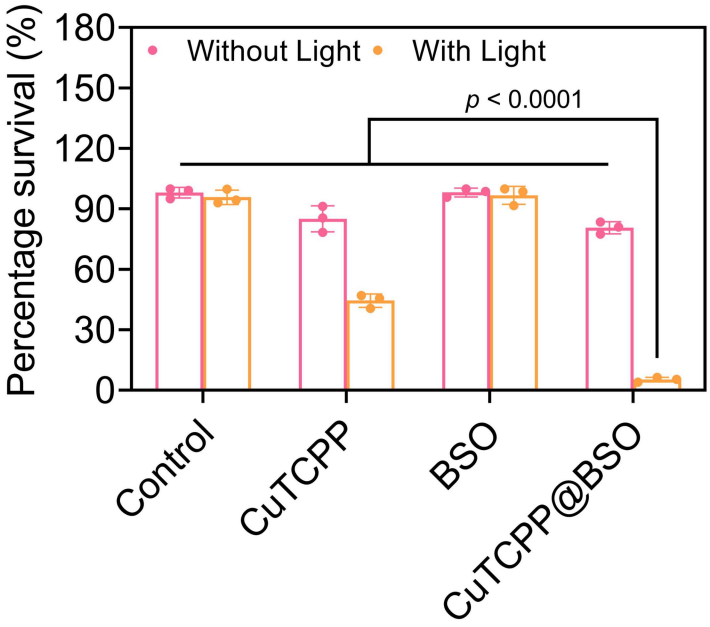

Fig. S6 Bacterial survival percentages derived from colony counts in Figure S2. Data are presented as mean ± SD (n=3). Statistical evaluation utilized two-way ANOVA with Tukey's post-hoc analysis.

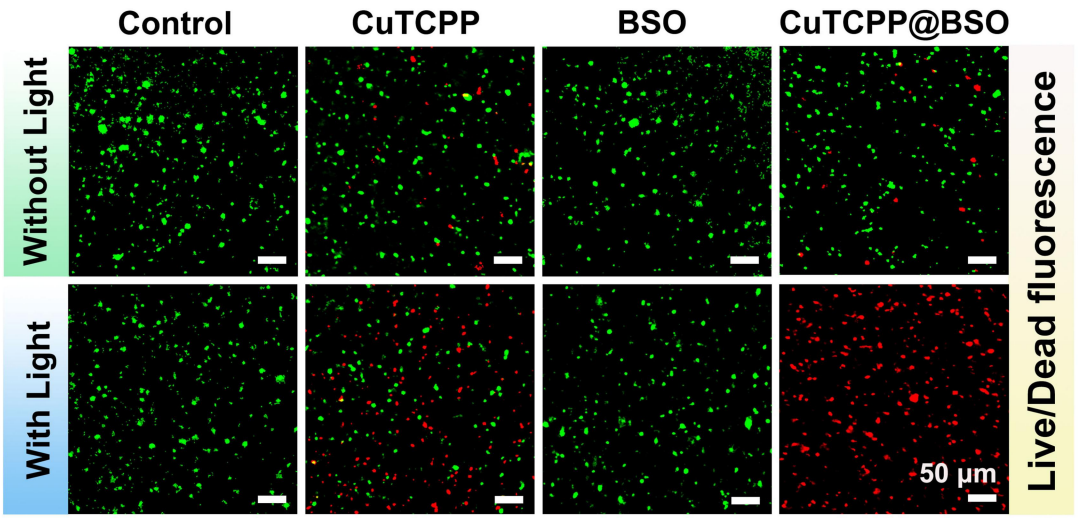

Fig. S7 Fluorescence images of *E. coli* stained with FDA (green, live) and PI (red, dead) post-treatment.

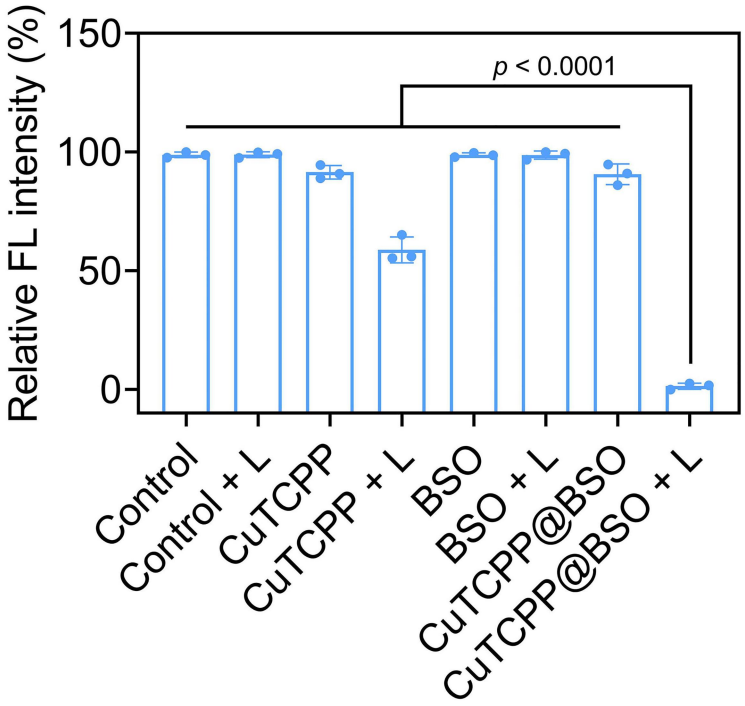

Fig. S8 The fluorescence intensity corresponding to live (green) *E. coli* cells in Figure S7 was quantified. Statistical analysis was conducted using one-way ANOVA with Tukey's test.

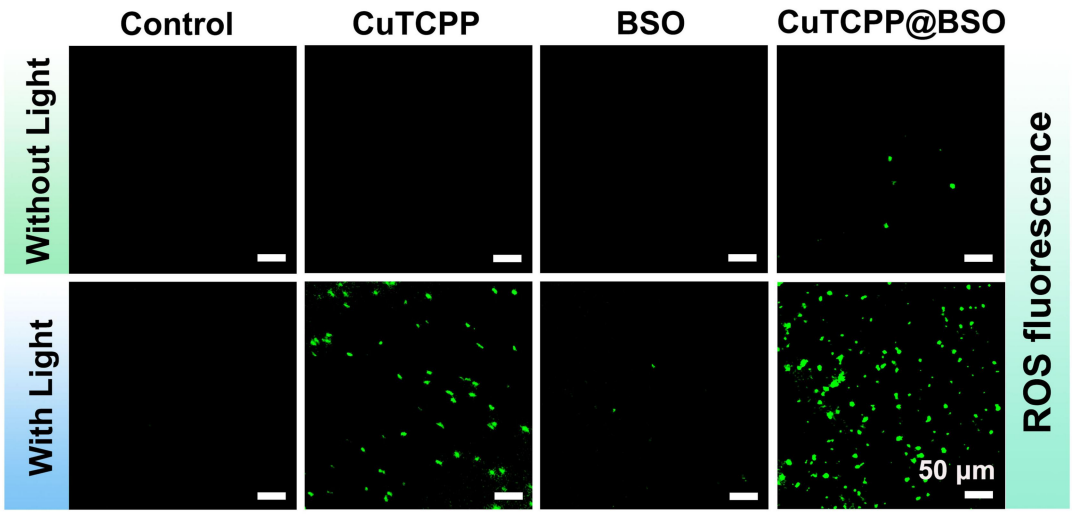

Fig. S9 Fluorescence micrographs illustrating the levels of intracellular ROS in *E. coli* across different treatment groups, detected by DCFH-DA.

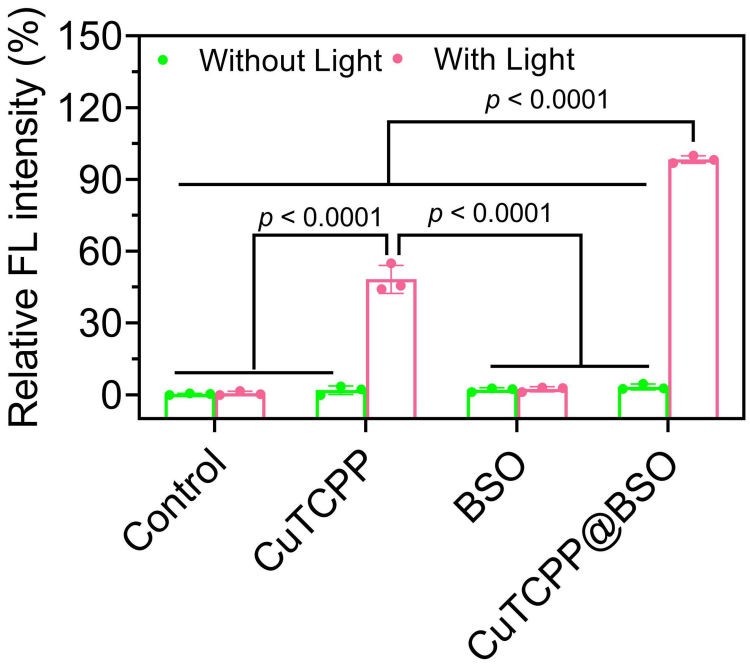

Fig. S10 Statistical analysis of the fluorescence intensity from the ROS imaging in Fig. S6, performed using two-way ANOVA with Tukey's post-hoc test.

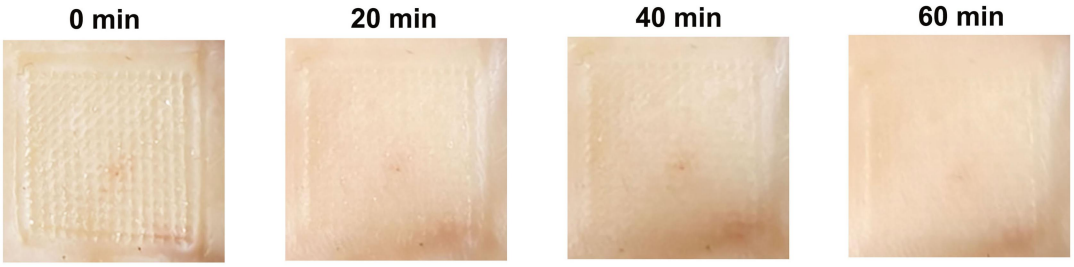

Fig. S11 Time-course images showing the disappearance of micro-pores on mouse skin following removal of MN/CuTCPP@BSO.

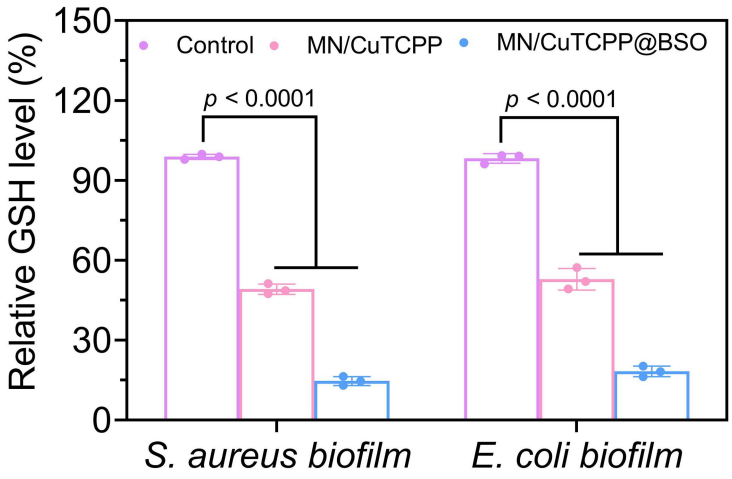

Fig. S12 Quantification of GSH depletion in *S. aureus* and *E. coli* biofilms following exposure to MN/CuTCPP or MN/CuTCPP@BSO. Data are presented as mean ± SD (n=3).

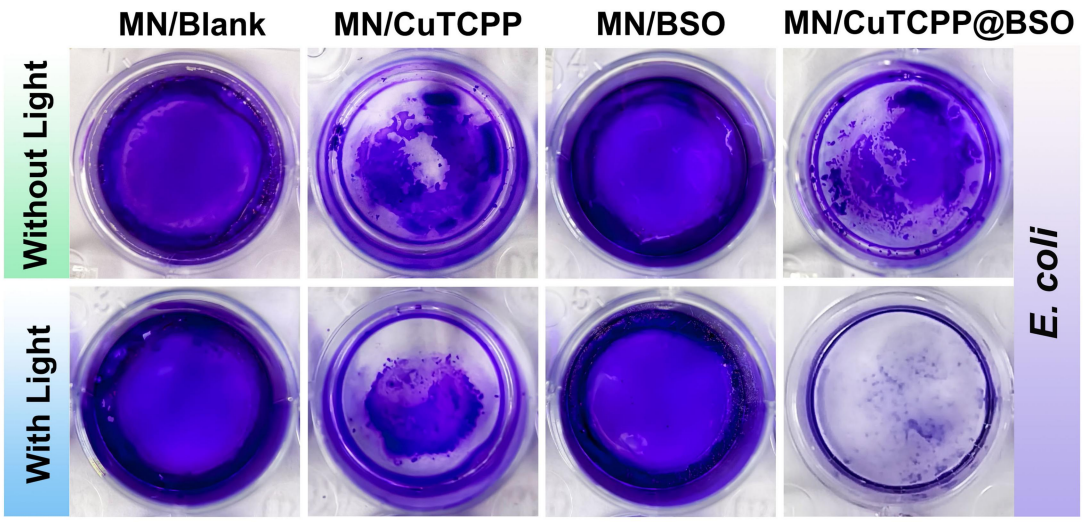

Fig. S13 Crystal violet staining of *E. coli* biofilm following treatment with different microneedle formulations.

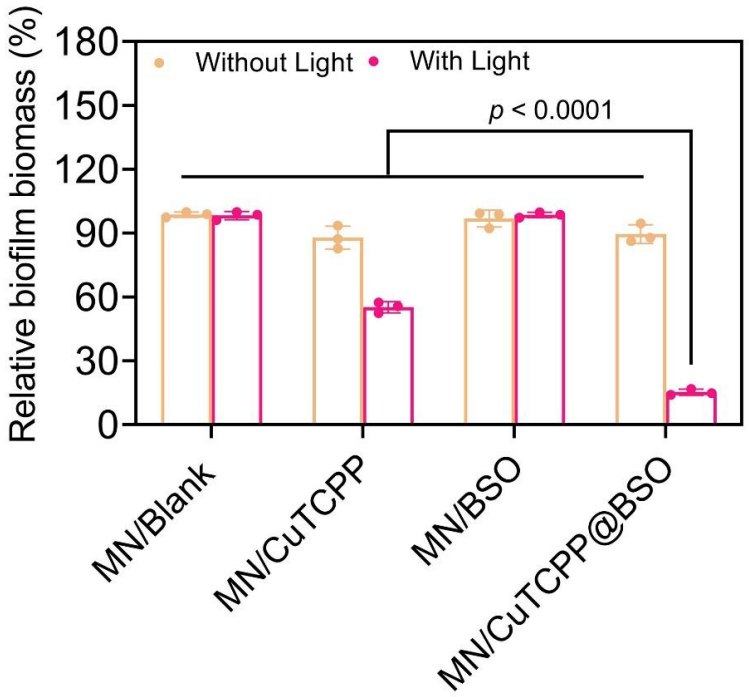

Fig. S14 Quantification of residual biomass for *E. coli* biofilm after various treatments. Statistical analysis was performed using two-way ANOVA with the Tukey post-test.

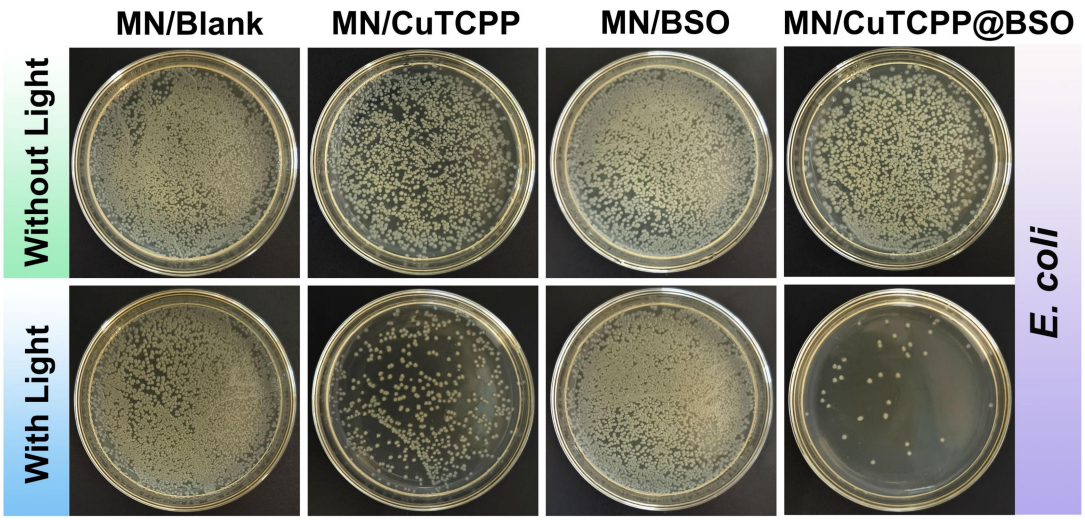

Fig. S15 Colonies of *E. coli* retrieved from biofilm and plated after different therapies.

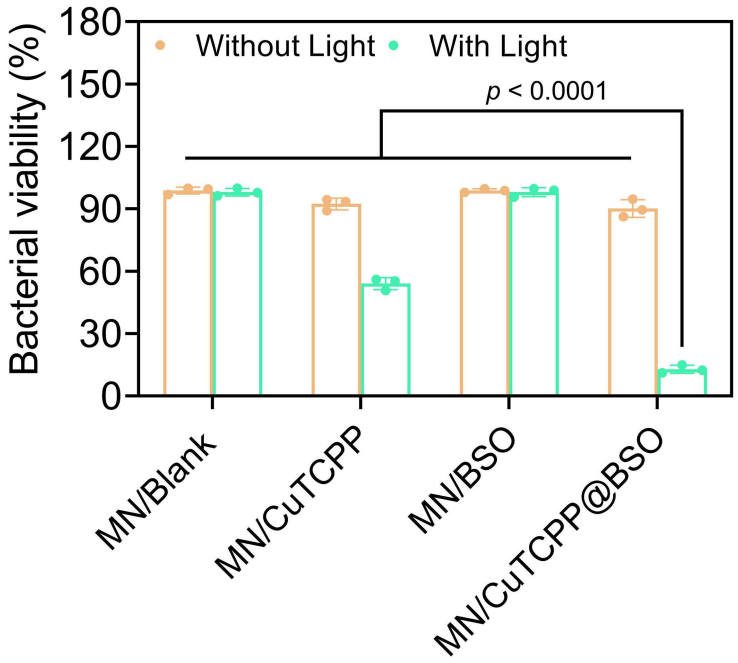

Fig. S16 Survival rates of *E. coli* isolated from biofilm post-treatment. Statistical analysis was conducted using two-way ANOVA, followed by the Tukey post-test.

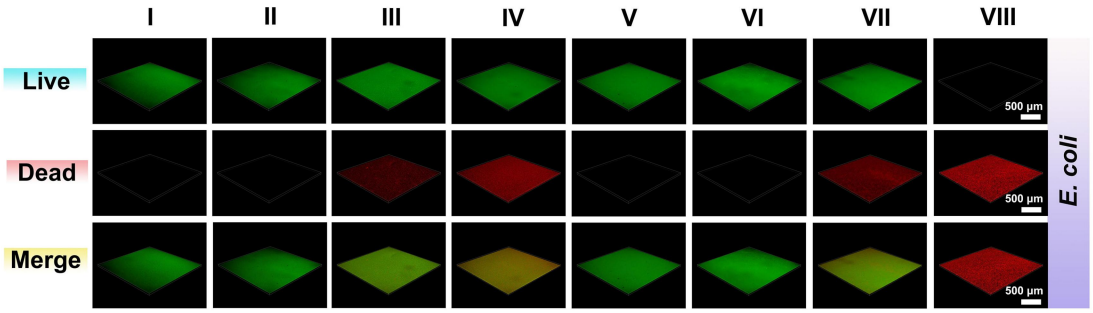

Fig. S17 3D-CLSM live/dead images of *E. coli* biofilm after exposure to different microneedles.

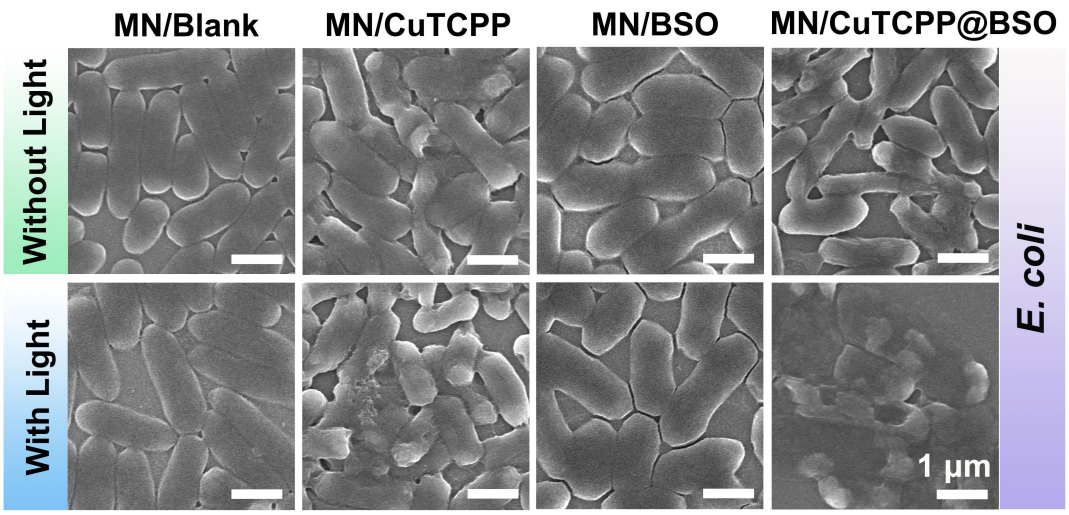

Fig. S18 SEM analysis showing morphological alterations in *E. coli* biofilm post-treatment.

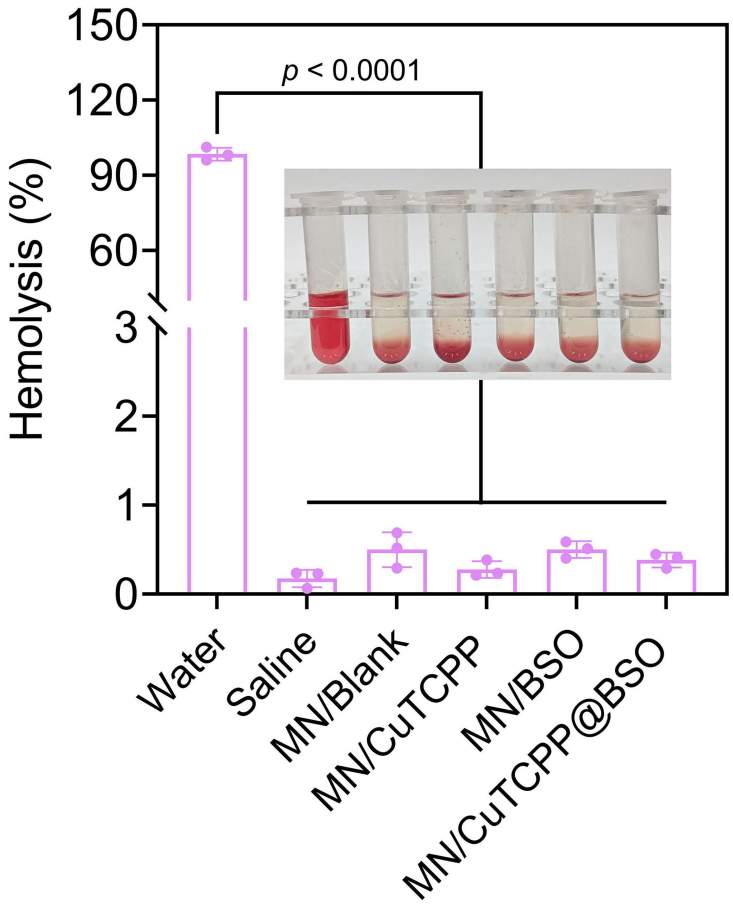

Fig. S19 Hemocompatibility assessment of microneedles with varying compositions. Statistical significance was determined by one-way ANOVA with Tukey's post hoc test.

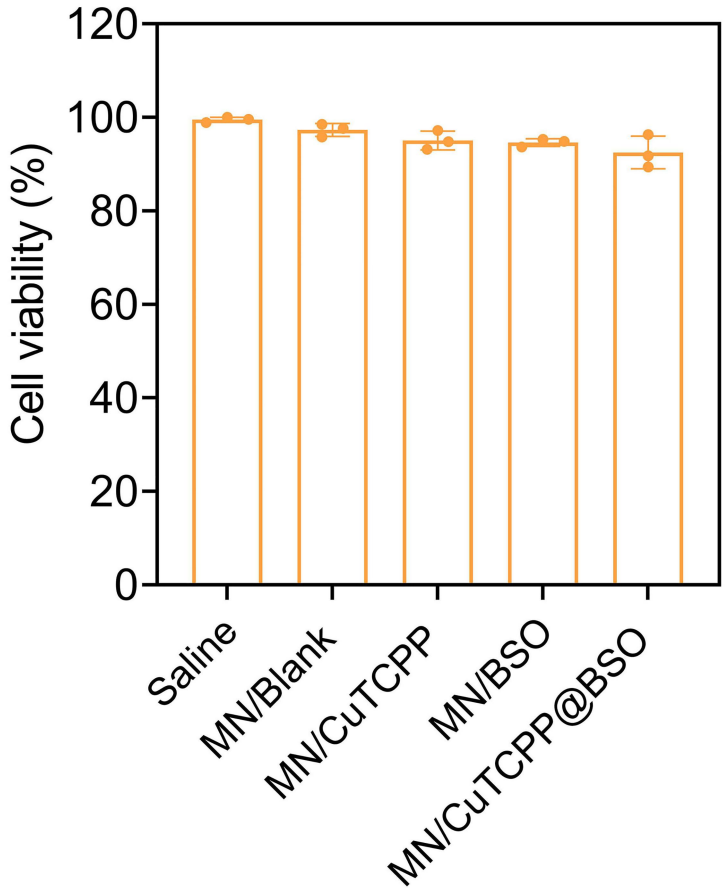

Fig. S20 Cytotoxicity evaluation of different microneedle formulations toward L929 fibroblasts *in vitro*.

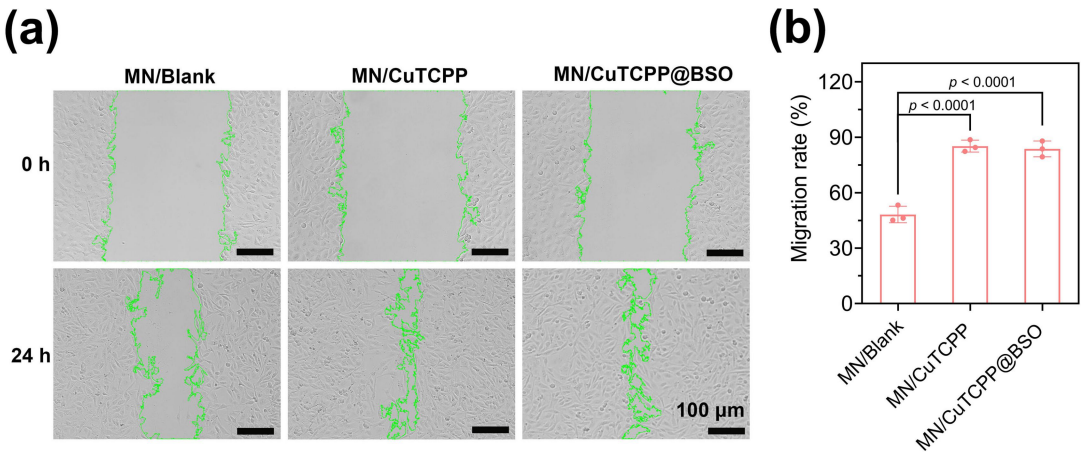

Fig. S21 Scratch assay assessing HUVEC migration *in vitro*. (a) Microscopic images of cell monolayers at 0 h and 24 h post-scratch under different treatments. (b) Quantified migration rates after 24 h (n = 3). Significance was evaluated by one-way ANOVA coupled with Tukey's post hoc analysis.

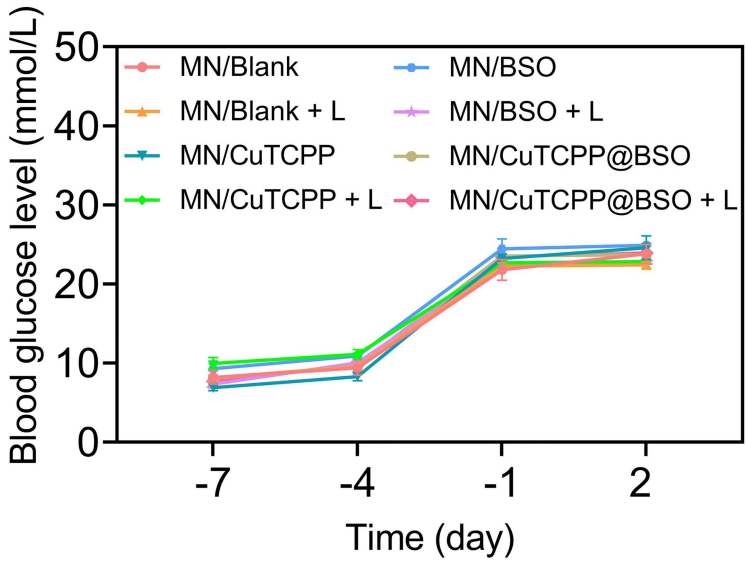

Fig. S22 Blood glucose monitoring following STZ injection.

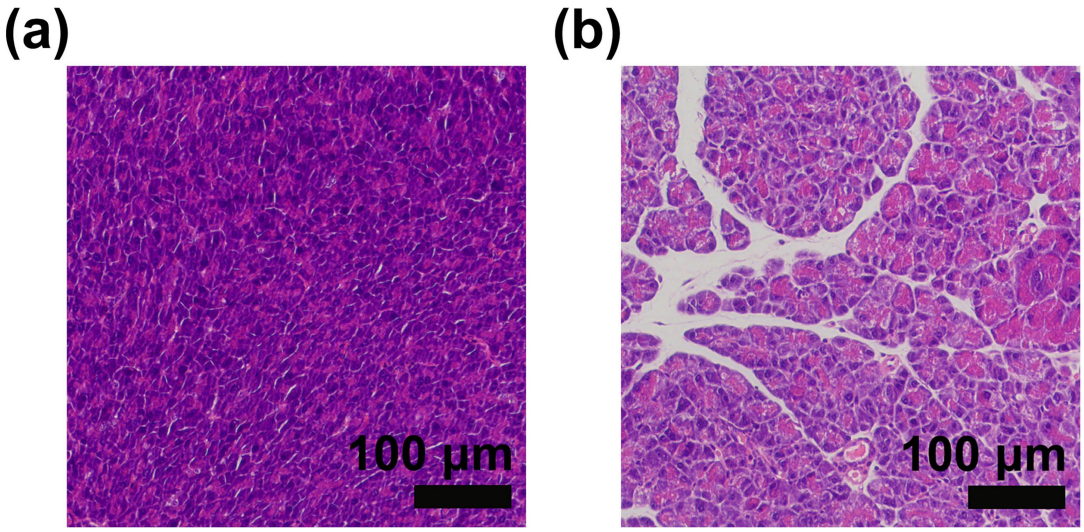

Fig. S23 (a) H&E-stained pancreas from a healthy mouse. (b) H&E-stained pancreas from a diabetic mouse, showing characteristic islet degeneration.

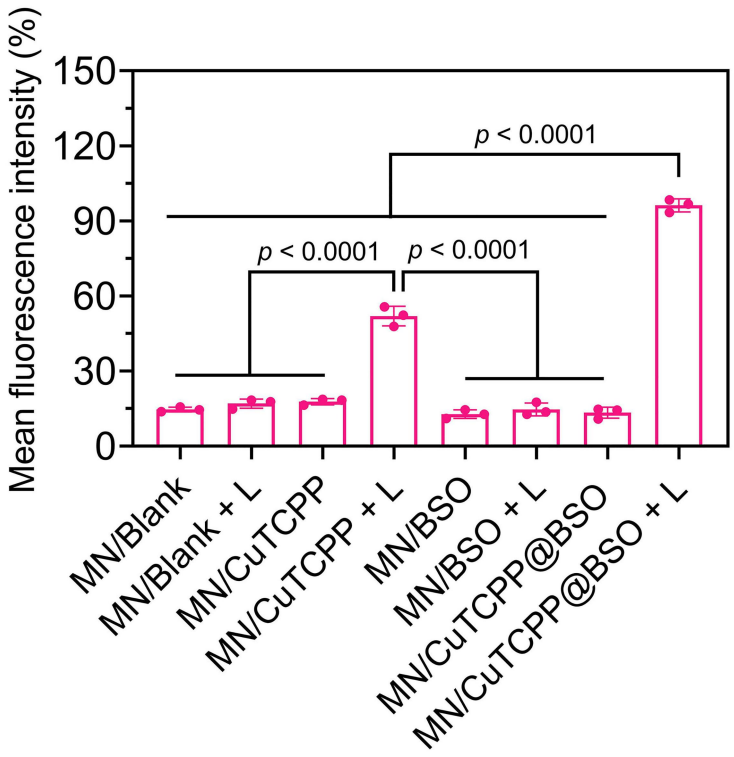

Fig. S24 Semi-quantitative analysis of the average fluorescence intensity of ROS at the wound site after different treatments.

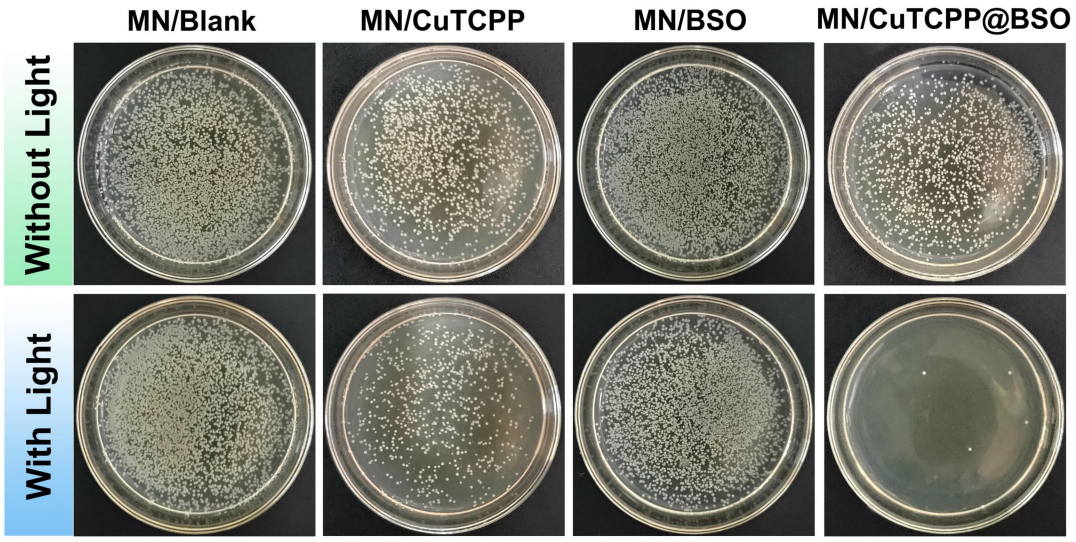

Fig. S25 Bacterial colony formation from wound tissues after treatment.

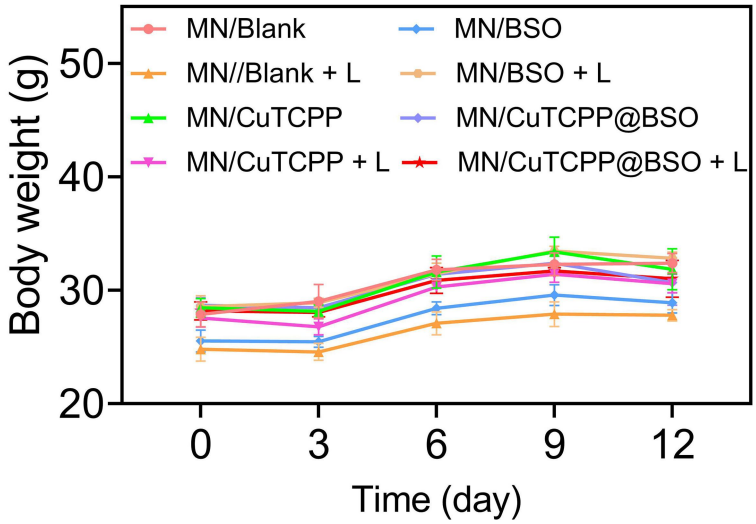

Fig. S26 Body weight progression of mice during the 12-day treatment period.